Ballistic-phonon heat conduction at the nanoscale as revealed by time-resolved x-ray diffraction and time-domain thermoreflectance

M. Highland, B. C. Gundrum, Yee Kan Koh, R. S. Averback, and David G. Cahill
Frederick Seitz Materials Research Laboratory and Department of Materials Science and Engineering, University of Illinois, Urbana, Illinois 61801, USA

V. C. Elarde and J. J. Coleman
Department of Electrical and Computer Engineering, University of Illinois, Urbana, Illinois 61801, USA

D. A. Walko and E. C. Landahl
Advanced Photon Source, Argonne National Laboratory, Argonne, Illinois 60439, USA
(Received 1 June 2007; revised manuscript received 16 July 2007; published 22 August 2007)

We use time-resolved measurements of the evolution of surface and buried layer temperatures to quantify the contribution of ballistic phonons to heat transport on nanometer length scales. A laser pulse heats a 100 nm thick Al film which cools by conduction into a GaAs substrate. The top 120–250 nm of the GaAs substrate is doped with In to create a buried layer with a distinct lattice constant. The cooling of the Al film is monitored by time-domain thermoreflectance and, in the second set of experiments, the heating and cooling of the GaAs:In buried layer are monitored by time-resolved x-ray diffraction. The combination of these data shows that thermal transport by ballistic phonons accounts for nearly 20% of the heat flow across the buried layer on nanosecond time scales.

DOI: 10.1103/PhysRevB.76.075337 PACS number(s): 66.70.+f, 65.40.−b

I. INTRODUCTION

In nonmetallic crystals, thermal transport is mediated by phonons with a wide distribution of wavelengths and lifetimes. If the characteristic length scale of a structure is large compared to the mean free paths of the phonons that contribute most strongly to the thermal conductivity, the diffusion equation is an accurate description of the transport of thermal energy. In nanoscale devices and structures, however, the diffusion equation is not a rigorous approach because the length and time scales of interest often overlap with the mean free paths and lifetimes of the dominant heat carriers,[1–5] i.e., a significant quantity of heat can be carried by a small fraction of phonons that are out of equilibrium with the majority of the vibrational modes that dominate the heat capacity of the solid. The heat current also becomes nonlocal in the temperature gradient.[6] The growing need to better understand heat transport at the nanoscale is driving the development of experimental techniques and theoretical models capable of probing and predicting thermal transport in this new regime.[7]

Time-domain thermoreflectance (TDTR) is a well established optical pump-probe technique that measures the evolution of surface temperature with picosecond time resolution.[8,9] Because of this high time resolution, TDTR is sensitive to the physics of heat conduction on nanometer length scales but, in practice, this sensitivity is limited by the geometry. TDTR measures the temperature at the surface and cannot access the evolution of temperature at other locations in the structure. Furthermore, while we have recently developed accurate methods for modeling TDTR data using analytical solutions of the heat diffusion equation,[10] it is not yet possible to quantify deviations from diffusive heat flow using TDTR alone.

For these reasons, we have developed an approach for probing the temperature evolution of buried layers on picosecond time scales by time-resolved x-ray diffraction (TRXRD). The combination of TDTR data for the decay of the surface temperature and TRXRD data for the heating and cooling of a buried layer provides a nearly complete picture of heat conduction at the nanoscale. We have applied this approach to thin film structures consisting of 120–250 nm layers of $(GaAs)_{1-x}(InAs)_x$ grown epitaxially on GaAs substrates and coated with a 100 nm film of Al. We find that a significant fraction of the heat that leaves the Al film is carried by a small number of phonon modes with mean free paths longer than the thickness of the buried $(GaAs)_{1-x}(InAs)_x$ layer. We refer to these phonons as "ballistic" phonons since they traverse the alloy layer without scattering. The ballistic phonons represent the nonequilibrium portion of the phonon population within the alloy layer, and since the ballistic phonons do not scatter within the alloy layer, they do not contribute to its heating.

Previous work using x rays to study phonon dynamics[11] applied diffuse x-ray scattering to probe photoexcited nonequilibrium phonon populations in GaAs. McWhan *et al.*[11] were able to set an upper bound of ~ 2 μs on the lifetime of zone boundary phonons. In our work, we have used x-ray diffraction with a time resolution of 100 ps to determine the fraction of heat carried by nonequilibrium phonon populations in $(GaAs)_{1-x}(InAs)_x$.

II. EXPERIMENTAL DETAILS

A. Sample preparation

The $(GaAs)_{1-x}(InAs)_x$ layers were grown in a vertical chamber, atmospheric pressure metal-organic chemical vapor

deposition (MOCVD) system from arsine, trimethyl gallium, and trimethyl indium precursors with a V/III ratio of ≈20. After a 10 min, 800 °C desorption bake of the semi-insulating GaAs (001) substrates, the temperature was ramped down to 625 °C for the deposition of a 100 nm GaAs buffer layer followed by the $(GaAs)_{1-x}(InAs)_x$ layer. We prepared three samples with compositions and thicknesses of the alloy layers close to but below the estimated critical thicknesses for strain relaxation.[12] As expected, high-resolution x-ray diffraction showed that the layers were fully strained. The $(GaAs)_{1-x}(InAs)_x$ layers were grown fully strained to eliminate phonon scattering by dislocations that would be present in partially relaxed $(GaAs)_{1-x}(InAs)_x$ layers. The composition of the samples was derived from the tetragonal strain assuming the validity of Vegard's law and a Poisson ratio of $\nu=0.31$.[13] After the samples were removed from the MOCVD system, a 100 nm thick film of Al was deposited in a separate chamber by magnetron sputtering. The thickness of the Al film was measured by picosecond acoustics.

B. Time-domain thermoreflectance and time-resolved x-ray diffraction

TDTR measurements used the apparatus and analysis methods described previously.[7,10] The pump and probe beam powers were 15 mW and the $1/e^2$ radii of the laser spots were 15 μm; the temperature rise created by this laser intensity was <2 K.[10]

TRXRD experiments on the same samples were performed at the sector 7 MHATT-XOR beamline at the Advanced Photon Source (APS) of Argonne National Laboratory. In the standard operation mode of the APS, 24 electron bunches circle the APS storage ring every 3.68 μs. An amplified Ti:sapphire pump laser with a repetition rate of ≈5 kHz is synchronized to the storage ring[14] and used to heat the surface of the sample. Laser pulses with energies of 280 or 110 μJ were focused to an elliptical spot on the sample with $1/e^2$ radii of 1.26 and 2.63 mm. The evolution of strain in the sample was probed by 100 ps, 9.2 keV x-ray pulses.[15] Each x-ray pulse contained $\sim 10^6$ photons in a spot 550 μm high and focused to 30–60 μm wide using an elliptical, grazing-incidence mirror. The large difference in the size of the x-ray and laser spots in this experiment ensures that heat flow across the layers can be treated as one dimensional. A gated x-ray detector measured the diffraction intensity generated by the x-ray pulse that arrived at the sample close in time to the laser pulse and the x-ray pulse that arrived 153 ns later. The temporal resolution of this measurement technique is limited by the 100 ps duration of the x-ray pulse; acoustic phenomena are therefore too short lived to be measured by the technique. Measurements of the GaAs (004) and the $(GaAs)_{1-x}(InAs)_x$ (004) diffraction peaks were performed with a four-circle diffractometer near a Bragg angle of 28.5°.

C. Relationship between the position of the diffraction peak and the temperature distribution of the buried layer

At long times, the temperature distribution $\Delta T(z)$ within the buried layer is homogeneous and the shift in the position of the x-ray diffraction peak of the buried layer can be easily calculated from the coefficient of thermal expansion α ($\alpha = 5.97 \times 10^{-6}$ K^{-1} for GaAs)[16] and Poisson ratio υ of the buried layer,

$$\frac{\Delta L}{L_0} = \alpha\left(\frac{1+\nu}{1-\nu}\right)\Delta T, \tag{1}$$

where L_0 is the unshifted peak position in reciprocal space and ΔL is the change in the peak position. At short times, however, $\Delta T(z)$ is not uniform and we must relate $\Delta T(z)$ to the changes in the position and shape of the intensity of the diffraction peak $I(\boldsymbol{K})$, where $\boldsymbol{K}$ is the scattering vector. We show below that for small values of $\Delta T(z)$, the shape of the diffraction peak is nearly constant and the main effect of $\Delta T(z)$ is a shift of the diffraction peak in reciprocal space $I(\boldsymbol{K}-\boldsymbol{s})$. What we desire is a function $G(z)$ that connects a δ function of strain at some location in the buried layer to a contribution to $\boldsymbol{s}$. The full $\boldsymbol{s}$ can then be calculated from the integral of $G(z)\Delta T(z)$.

Since we are only concerned with the change in the position of a $(00L)$ reflection in the direction normal to the surface, the diffraction problem reduces to a one-dimensional integral transform over the thickness of the layer. We define $z=0$ as the center of the buried layer. The x-ray absorption depth is much larger than the thickness h of the buried layer; therefore, $G(z)$ is an even function of z and we can simplify the calculation of $G(z)$ by introducing two delta functions of strain at positions $z=a$ and $z=-a$. The scattering amplitude from the layer is then

$$A(k) = \int_{-h/2}^{-a} \exp(-i\delta)\exp(ikz)dz + \int_{-a}^{a} \exp(ikz)dz + \int_{a}^{h/2} \exp(i\delta)\exp(ikz)dz, \tag{2}$$

where δ is the strength of the δ function of strain and

$$k = 2\pi \boldsymbol{K}\cdot\hat{z}. \tag{3}$$

For small δ,

$$A(k) = \int_{-h/2}^{h/2} \exp(ikz)dz - i\delta\int_{-h/2}^{-a} \exp(ikz)dz + i\delta\int_{a}^{h/2} \exp(ikz)dz, \tag{4}$$

which simplifies to

$$A(k) = \frac{2\sin(kh/2)}{k} - \frac{2\delta}{k}(\cos(kh/2) - \cos(ka)). \tag{5}$$

Equation (5) describes the amplitude of the diffraction from a thin layer as a function of the location $z=a$ of a symmetrical δ function of strain. Equation (5) does not describe a simple rigid shift of the diffraction peak. However, the changes in amplitude are approximately the same as would be produced by a shift $\boldsymbol{s}$ in the position of the diffraction peak. Near $kh=\pi$, this shift is

$$\boldsymbol{s} = \frac{\delta}{\pi h}\cos\left(\frac{\pi a}{h}\right)\hat{z}. \tag{6}$$

The key result is the cosine dependence on the position of the strain. Normalizing this cosine function over the thickness of the layer gives the appropriate weighting function

$$G(z) = \frac{\pi}{2h}\cos\left(\frac{z}{h}\pi\right). \tag{7}$$

The weighted average temperature of the layer is

$$\Delta T_{av} = \int_{-h/2}^{h/2} G(z)\Delta T(z)dz, \tag{8}$$

and for an arbitrary temperature distribution within a buried layer, the shift in the position of the diffraction peak is

$$\frac{\Delta L}{L_0} = \alpha\left(\frac{1+\nu}{1-\nu}\right)\Delta T_{av}. \tag{9}$$

Since the shape of the diffraction peak is known, we can invert Eq. (9) and use the changes in intensity measured at the half-maximum position to determine the average temperature ΔT_{av} of the buried alloy layer as a function of delay time t.

III. RESULTS

A. Time-domain thermoreflectance

Figure 1 shows the raw data for the ratio of the in-phase and out-of-phase signals measured by the rf lock-in amplifier used in the TDTR experiments. The dashed line in Fig. 1 shows a fit of the data using a diffusive heat flow model.[10] The thermal conductivity Λ of the $(GaAs)_{1-x}(InAs)_x$ layer and the thermal conductance G of the Al-$(GaAs)_{1-x}(InAs)_x$ interface are the only two free parameters. This diffusive heat flow model is an exact numerical solution of the heat diffusion equation in cylindrical coordinates and, therefore, radial heat flow within the Al films and the sample is fully taken into account.

The solid line in Fig. 1 is a fit to the data using a thermal model in which an additional channel for heat flow is used to model ballistic heat transport across the buried layer. The thermal effusivity ε of the second channel is the third free parameter in this two-channel model. This two-channel model is described in detail below.

B. Time-resolved x-ray diffraction

Figure 2 shows an example of the change in the diffraction from a $(GaAs)_{1-x}(InAs)_x$ strained layer at a positive value and a negative value for the time delay t between the laser pump and x-ray probe. To record how the strain in the sample varies as a function of t and to make the most effective use of x-ray beam time, we do not measure the diffraction intensity as a function of both diffraction angle and t but instead fix the diffraction angle at the half-maximum position and vary only t. To calculate the average temperature of the film from the measured change in intensity, we first fit the

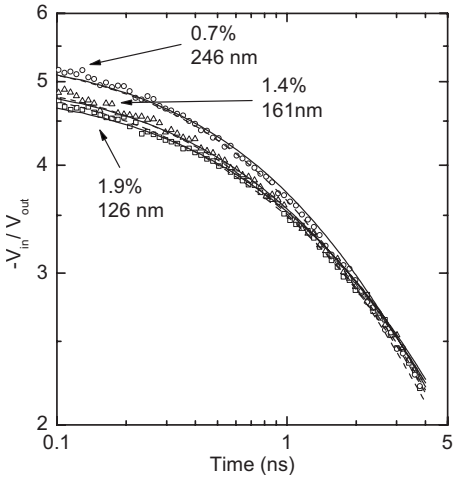

FIG. 1. The ratio of the in-phase and out-of-phase signals from the rf lock-in amplifier used in TDTR measurements versus delay time between the pump and probe laser pulses for the 246 nm $(GaAs)_{0.993}(InAs)_{0.007}$, 161 nm thick $(GaAs)_{0.986}(InAs)_{0.014}$ layer, and 126 nm $(GaAs)_{0.981}(InAs)_{0.019}$ samples. The dashed lines are fits of the data using a one-channel heat flow model in which the thermal conductivity of the $(GaAs)_{1-x}(InAs)_x$ layers and the thermal conductance of the Al-$(GaAs)_{1-x}(InAs)_x$ interfaces are free parameters. The solid lines are fits of the data using a two-channel heat flow model which accounts for both diffusive and ballistic heat flows. In the two-channel model, the effusivity of the second channel is an additional free parameter.

unshifted intensity of the $(GaAs)_{1-x}(InAs)_x$ (004) diffraction peak with a Gaussian function,

$$I(L) = I_0 + \left(\frac{A}{w\sqrt{\pi/2}}\right)\exp\left(-2\left(\frac{L-L_0}{w}\right)^2\right). \tag{10}$$

This Gaussian function is then inverted to describe peak position as a function of intensity at a single point in time,

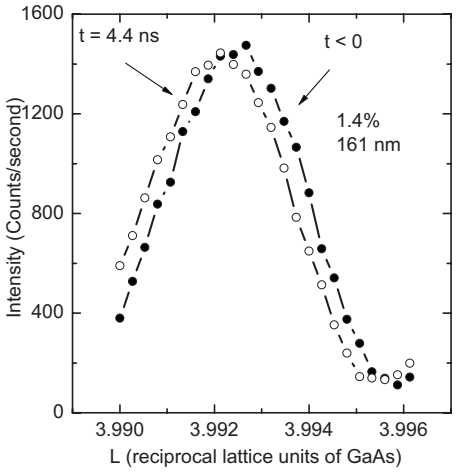

FIG. 2. Two scans of the 004 x-ray diffraction peak from a thin layer with composition $(GaAs)_{0.986}(InAs)_{0.014}$. The filled circles show the diffraction peak before the arrival of the laser pulse and the open circles show the diffraction peak 4.4 ns after the laser pulse has reached the sample.

$$\frac{(L-L_0)}{L_0} = \frac{w}{L_0}\left[-\frac{1}{2}\ln\left(\frac{w\sqrt{\pi/2}(I-I_0)}{A}\right)\right]^{1/2}. \quad (11)$$

As the layer is heated, the diffraction peak will shift as a function time. We calculate the peak shift from the change of intensity as a function of time $\Delta I(t)$ with the relation

$$\frac{\Delta L(t)}{L_0} = \frac{w}{L_0}\left[-\frac{1}{2}\ln\left(\frac{w\sqrt{\pi/2}(\Delta I(t))}{A}\right)\right]^{1/2}. \quad (12)$$

Substituting Eq. (12) into Eq. (9) and solving for ΔT_{av} yields the average temperature as a function of time, as shown by the data points in Fig. 3.

The dashed lines in Fig. 3 are the evolution of T_{av} of the buried layer predicted by a solution to the diffusion equation using the values of Λ and G measured using a one-channel model fit of the TDTR data. Since we do not know the laser fluence precisely, we adjust the laser fluence in the model to fit the model to the data at long times ($t > 150$ ns) where the temperature excursion is controlled solely by the known thermal effusivity of the GaAs substrate. The adjusted values for the laser fluence differ from predicted values by as much as a factor of ~2. We see that the heating rate and peak temperature predicted by the model exceed the temperature response measured by TRXRD. The solid line in Fig. 3 shows a fit of the TRXRD data using a two-channel thermal model with the same values of Λ, G, and ε used to generate the solid line in Fig. 1. The two-channel heat flow model is discussed in detail below.

Our use of the thermal expansion of the buried layer as a thermometer is justified because the vast majority of the phonons are in equilibrium and this equilibrium population of phonons determines the lattice expansion of the film. The small fraction of phonons that traverse the buried layer ballistically is not in equilibrium. The ballistic phonons make a significant contribution to the heat transport, but since all of the vibrational modes of the solid have Grüneisen parameters on the order of unity[17] and therefore contribute equally to the lattice expansion of the film, the contribution of the small number of ballistic phonons to the lattice expansion is negligible.

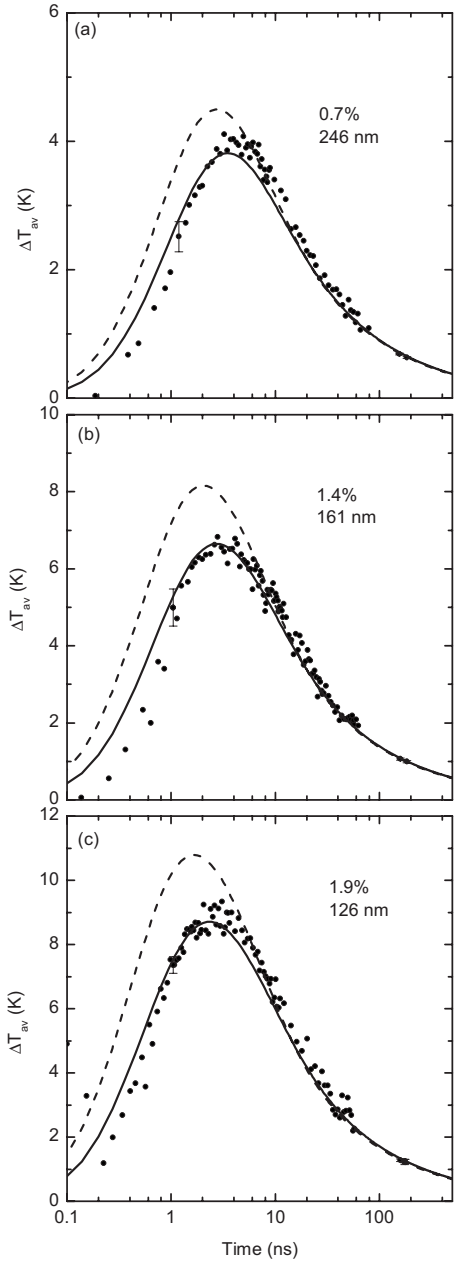

FIG. 3. The time evolution of the average temperature of (a) the 246 nm $(GaAs)_{0.993}(InAs)_{0.007}$ layer, (b) the 161 nm thick $(GaAs)_{0.986}(InAs)_{0.014}$ layer, and (c) the 126 nm $(GaAs)_{0.981}(InAs)_{0.019}$ layer as determined from shifts of the diffraction peak, see Eq. (12). The dashed lines are the evolution of the weighted average temperature of the buried layer predicted by a solution to the diffusion equation using the values of Λ and G measured using a one-channel model to fit the TDTR data. The solid lines are fits of the data using a two-channel heat flow model in conjunction with TDTR data to determine Λ, G, and ε.

IV. DISCUSSION

A. One- and two-channel heat flow models

The single channel thermal model used to generate the dashed lines shown in Figs. 1 and 3 uses solutions of the heat diffusion equation to calculate the temperature evolution of surface or buried layers. The single channel model treats the thermal conductivity of the $(GaAs)_{1-x}(InAs)_x$ layer Λ and the Al-$(GaAs)_{1-x}(InAs)_x$ interface conductance G as free parameters. As can be seen from Fig. 3, the single channel heat flow model does not yield a consistent value for G when used to fit both the TDTR and TRXRD data. This discrepancy can be attributed to the simplifying assumption in the single channel model that the cooling of the layers is governed by only diffusive heat flow. To reconcile the discrepancy in the values of G measured with TDTR and TRXRD, we have developed a thermal model in which heat propagates from the surface of a sample into the substrate via two distinct channels, simulating diffusive and ballistic heat flows, respectively.

The diffusive heat flow channel is modeled as before with the known thicknesses and heat capacities of the Al-$(GaAs)_{1-x}(InAs)_x$ layers, leaving the thermal conductivity

of the alloy layer Λ and the thermal conductance G of the interface between the Al film and the alloy layer as the two free parameters. Recall that our definition of a ballistic phonon is a phonon with a mean free path larger than the thickness of the alloy layer. Of course, the same phonon modes that are ballistic on the length scale of the thickness of the alloy layer are diffusive at depths in the GaAs substrate greater than the mean free path. Since we cannot currently incorporate ballistic transport directly into our thermal models, we approximate the contribution of ballistic phonons to the heat transport by a thin surface layer where the heat is deposited and a thick second layer with a high thermal diffusivity and low thermal effusivity. We refer to this second channel for heat transport as a "ballistic channel," in reference to the ballistic transport through the alloy layer, even thought the transport on longer length scales is diffusive in the substrate. The amount of heat carried by the ballistic channel is characterized by the effusivity ε of the second layer, which is defined as

$$\varepsilon = (\Lambda_2 C_2)^{1/2}, \tag{13}$$

where Λ_2 and C_2 are the thermal conductivity and heat capacity per unit volume of the second channel. To better characterize the two-channel model, we examine the sensitivity of the TDTR and TRXRD data to Λ, G, and ε of the ballistic channel in the next section.

B. Sensitivity parameters

We define the sensitivity of TDTR by[18]

$$S_{TDTR} = \partial \ln(-V_{in}/V_{out})/\partial \ln(\phi), \tag{14}$$

where V_{in} and V_{out} are the in-phase and out-of-phase voltage signals measured by the rf lock-in amplifier and ϕ is the thermal property of interest, in this case either Λ, G, or ε. Because the temperature excursion measured by TRXRD is small at short delay times t, we define a slightly different sensitivity as

$$S_{TRXRD} = \frac{\Delta T_{av}(t)}{\Delta T_{av\_peak}} (\partial \ln(\Delta T_{av}(t))/\partial \ln(\phi)), \tag{15}$$

where $\Delta T_{av}(t)$ is the temperature rise of the buried layer as a function of time and ΔT_{av_peak} is the peak average temperature excursion. Figure 4 shows the calculated sensitivities of the two techniques to the three free parameters listed above. The sensitivities of the TDTR measurement to both G and ε are similar in shape, indicating that the TDTR measurement cannot distinguish between ε and G. However, at short time ($t < \sim 1$ ns) the sensitivity of the TRXRD measurement is dominated by G and the sensitivity to G has a shape which is distinct from that of the sensitivity to ε, indicating that accurate values for G can be measured by fitting the TRXRD data at short times. Figure 4 also shows that the sensitivity of the TDTR measurement to both G and ε falls to zero near 1 ns, indicating that Λ can be determined from this point in the TDTR curve. Once Λ and G are fixed, ε can be measured by determining which value of ε simultaneously gives the best fit of the TRXRD and TDTR data near 2–3 ns.

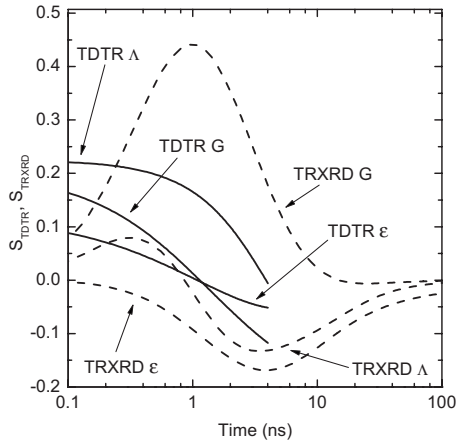

FIG. 4. Sensitivity [see Eqs. (14) and (15)] of the TDTR (solid lines) and TRXRD data (dashed lines) to the $(GaAs)_{1-x}(InAs)_x$ layer thermal conductivity Λ, the thermal conductance G of the Al-$(GaAs)_{1-x}(InAs)_x$ interface, and the effusivity ε of the ballistic channel plotted as a function of the delay time between pump and probe. This calculation was based on typical values of the three free parameters, $G=100$ MW m^{-2} K^{-1}, $\Lambda=15$ W m^{-1} K^{-1}, and $\varepsilon=1150$ J m^{-2} K^{-2} s$^{-1/2}$.

The inability of TDTR to distinguish between heat flow in a ballistic channel and a larger value of the Al-$(GaAs)_{1-x}(InAs)_x$ interface conductance is due to the fact that TDTR measures the evolution of the surface temperature of a sample. On the time scales relevant to this experiment, phonons in the Al layer are in equilibrium. As the Al film cools, phonons that traverse the alloy layer ballistically and deposit heat directly into the GaAs substrate have the same effect on the TDTR measurement as high values for the Al-$(GaAs)_{1-x}(InAs)_x$ interface conductance. On the other hand, TRXRD measures the lattice thermal expansion, which measures the temperature of the majority of vibrational modes that are in equilibrium and carry heat from the Al film into the $(GaAs)_{1-x}(InAs)_x$ layer. Since the heat carried by phonons that traverse the alloy layer ballistically will not contribute significantly to the expansion of the layer,[19] TRXRD is able to distinguish between G and ε. This difference in the sensitivity of the techniques makes the measurement of ballistic heat flow with a combination of TDTR and TRXRD possible.

C. Thermal conductivity, interface thermal conductance, and the effusivity of the ballistic channel

The values of Λ (filled circles) and G (open triangles) extracted from fitting the TDTR and TRXRD data with a two-channel heat flow model are summarized in Fig. 5. The measured thermal conductivities agree well with predictions of a lattice dynamics model following the approach of Morelli *et al.*,[20] also shown in Fig. 5. In the lattice dynamics model, we calculate the thermal conductivity using the Debye-Callaway formalism but treat the longitudinal and transverse modes separately. We assume that the phonon dispersion is isotropic and approximate the cutoff frequencies by the acoustic phonon frequencies at the zone boundary of

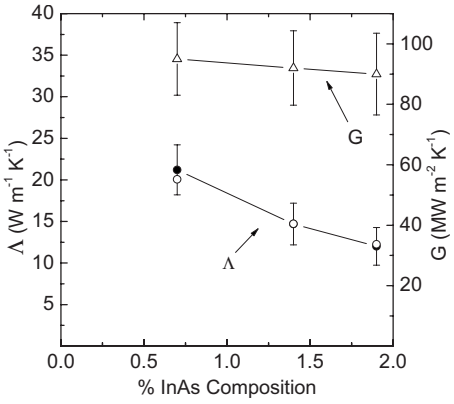

FIG. 5. Thermal conductivity (filled circles) of the $(GaAs)_{1-x}(InAs)_x$ layers and thermal conductance (open triangles) of the Al-$(GaAs)_{1-x}(InAs)_x$ interfaces for three samples as measured by TDTR and TRXRD versus percentage of InAs content. These values were extracted using a two-channel heat flow model. Also shown are predicted values (open circles) for the thermal conductivity of the $(GaAs)_{1-x}(InAs)_x$ layers based on the lattice dynamics model described in Sec. IV C. For the sample with 1.4% InAs content, the points for the measured and predicted values of the thermal conductivity overlap.

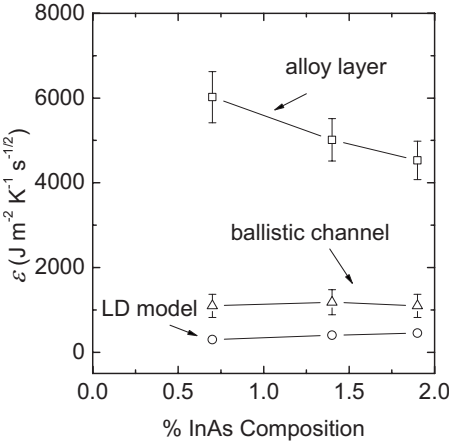

FIG. 6. The thermal effusivity of the ballistic heat flow channel (open triangles) used in the two-channel heat flow model to consistently fit both the TDTR and the TRXRD data plotted as a function of the percentage of the InAs content of the buried layer. Predicted values for the thermal effusivity of the ballistic channel based on the lattice dynamics model (LD model) described in Sec. IV C are plotted as open circles. The effusivity of the diffusive channel calculated from the full heat capacity of the alloy layer and the thermal conductivity of the alloy layer are plotted as open squares.

GaAs along [100].[21] As we have done previously,[22] we deviate from the approach of Ref. 20 and substitute a high temperature form for the *N*-process relaxation rate $\tau_N^{-1} = B_N \omega^2 T$. We fix the relative anharmonic scattering strengths of umklapp and normal processes, B_U and B_N, by the ratios of the mode velocities, Grüneisen constants, and cutoff frequencies, and obtain absolute values of the anharmonic scattering strengths from a fit to the thermal conductivities of GaAs.[23] We calculate the strength of Rayleigh scattering of our samples (lightly doped GaAs) using the dimensionless parameter Γ [see Eq. (16) of Ref. 20] that describes the strength of phonon scattering by mass disorder. We do not consider Rayleigh scattering by the differences in atomic size or bond strength because these contributions to Γ should oppose each other so that the total correction to Γ is relatively small.[21] We derive $\Gamma = Ax$, where x is the InAs content in our layers and $A = 0.19$. In our model, we include a boundary scattering length equal to the layer thickness, which accounts for the reduction in the thermal conductivity due to the finite film thickness.

To quantify the contribution of ballistic phonons to the total thermal transport from the Al film, we compare the thermal effusivity of the ballistic channel and the thermal effusivity of the alloy layers in Fig. 6. For layers with thicknesses of 246, 161, and 126 nm, the effusivity of the ballistic channel is 15%, 19%, and 19% of the total thermal effusivity, respectively.

We also used the same lattice dynamics model as described above to predict the effusivity of the ballistic channel. In this calculation, a phonon is considered to be ballistic if the mean free path is longer than the thickness of the buried layer. The results of those calculations are included in Fig. 6. The predicted effusivities are approximately a factor of 4 less than the measured values.

We compared the temperature of the Al film on the 126 nm alloy layer 1 ns after heating using fixed values for G and Λ with and without the ballistic heat flow channel present. After 1 ns of cooling, the temperature of the Al was 20% lower when the ballistic channel was present, which indicates that 20% of the heat leaving the Al layer was carried by the ballistic channel.

V. CONCLUSION

We have shown that with a combination of TRXRD and TDTR, we are able to measure the contribution of ballistic phonons to thermal transport across films with thicknesses of ~100 nm. We have developed a heat flow model which accounts for both diffusive and ballistic heat flows and is therefore capable of fitting both the TDTR and TRXRD measurements.

ACKNOWLEDGMENTS

This work was supported by DOE Grant No. DEFG02-91ER45439. Sample characterization used the Central Facilities of the Frederick Seitz Materials Research Laboratory at UIUC which is partially supported by DOE Grant No. DEFG02-91ER45439. Use of the Advanced Photon Source was supported by the U.S. Department of Energy, Office of Science, Office of Basic Energy Sciences, under Contract No. DE-AC02-06CH11357.

[1] Y. S. Ju and K. E. Goodson, Appl. Phys. Lett. **74**, 3005 (1999).
[2] M. Ashegi, Y. K. Leung, S. S. Wong, and K. E. Goodson, Appl. Phys. Lett. **71**, 1798 (1997).
[3] A. A. Joshi and A. Majumdar, J. Appl. Phys. **74**, 31 (1993).
[4] G. Chen, Phys. Rev. B **57**, 14958 (1998).
[5] D. Li, Y. Wu, P. Kim, L. Shi, P. Yang, and A. Majumdar, Appl. Phys. Lett. **83**, 2934 (2003).
[6] G. D. Mahan and F. Claro, Phys. Rev. B **38**, 1963 (1988).
[7] D. G. Cahill, W. K. Ford, K. E. Goodson, G. D. Mahan, A. Majumdar, H. J. Maris, R. Merlin, and S. R. Philpot, J. Appl. Phys. **93**, 793 (2003).
[8] C. A. Paddock and G. L. Eesley, J. Appl. Phys. **60**, 285 (1986).
[9] R. J. Stoner and H. J. Maris, Phys. Rev. B **48**, 16373 (1993).
[10] D. G. Cahill, Rev. Sci. Instrum. **75**, 5119 (2004).
[11] D. B. McWhan, P. Hu, M. A. Chin, and V. Narayanamurti, Phys. Rev. B **26**, 4774 (1982).
[12] J. W. Matthews and A. E. Blakeslee, J. Cryst. Growth **27**, 118 (1974).
[13] T. B. Bateman, H. J. McSkimin, and J. M. Whelan, J. Appl. Phys. **30**, 544 (1959).
[14] M. F. DeCamp, D. A. Reis, D. M. Fritz, P. H. Bucksbaum, E. M. Durfresne, and R. Clarke, J. Synchrotron Radiat. **12**, 177 (2005).
[15] S. H. Lee, Ph.D. thesis, University of Michigan, 2006.
[16] S. I. Novikova, Sov. Phys. Solid State **3**, 129 (1961).
[17] T. Soma and K. Kudo, J. Phys. Soc. Jpn. **48**, 115 (1980).
[18] B. C. Gundrum, D. G. Cahill, and R. S. Averback, Phys. Rev. B **72**, 245426 (2005).
[19] G. Chen, J. Heat Transfer **124**, 320 (2002).
[20] D. T. Morelli, J. P. Heremans, and G. A. Slack, Phys. Rev. B **66**, 195304 (2002).
[21] K. Kunc, Ann. Phys. (Paris) **8**, 319 (1973).
[22] D. G. Cahill, F. Watanabe, A. Rockett, and C. B. Vining, Phys. Rev. B **71**, 235202 (2005).
[23] M. G. Holland, Phys. Rev. **134**, A471 (1964).